Icarus xxx (2012) xxx–xxx

Contents lists available at SciVerse ScienceDirect

Icarus

journal homepage: www.elsevier.com/locate/icarus

The characteristics of the O_2 Herzberg II and Chamberlain bands observed with VIRTIS/Venus Express

A. Migliorini [a,*], G. Piccioni [a], J.C. Gérard [b], L. Soret [b], T.G. Slanger [c], R. Politi [a], M. Snels [d], P. Drossart [e], F. Nuccilli [a]

[a] IAPS-INAF, via del Fosso del Cavaliere, 100, 00133 Rome, Italy
[b] LPAP, ULg, Allée du 6 Août, 17 – Sart Tilman, B-4000 Liège, Belgium
[c] MPL, SRI International, Menlo Park, CA, United States
[d] ISAC/CNR, via del Fosso del Cavaliere, 100, 00133 Rome, Italy
[e] LESIA, 5, place Jules Janssen, 92195 Meudon, Paris, France

ARTICLE INFO

Article history:
Available online xxxx

Keyword:
Venus
Venus Atmosphere
Spectroscopy

ABSTRACT

The oxygen Venus nightglow emissions in the visible spectral range have been known since the early observations from the Venera spacecraft. Recent observations with the VIRTIS instrument on board Venus Express allowed us to re-examine the Herzberg II system of O_2 and to further study its vertical distribution, in particular the (0–v'' with v'' = 7–13) bands. The present work describes the vertical profile of the observed bands and relative intensities from limb observation data. The wavelength-integrated intensities of the Herzberg II bands, with v'' = 7–11, are inferred from the recorded spectra. The resulting values lie in the range of 84–116 kR at the altitudes of maximum intensity, which are found to lie in the range of 93–98 km.

Three bands of the Chamberlain system, centered at 560 nm, 605 nm, and 657 nm have been identified as well. Their emission peak is located at about 100 km, 4 km higher than the Herzberg II bands.

For the first time, the O_2 nightglow emissions were investigated simultaneously in the visible and in the IR spectral range, showing a good agreement between the peak position for the Herzberg II and the $O_2(a^1\Delta_g–X^3\Sigma_g^-)$ bands. An airglow model, proposed by Gérard et al. (Gérard, J.C., Soret, L., Migliorini, A., Piccioni, G. [2012]. Icarus.) starting from realistic O and CO_2 vertical distributions derived from Venus-Express observations, allows reproduction of the observed profiles for the three O_2 systems.

1. Introduction

The oxygen emissions in the 300–700 nm spectral range, known as the $O_2(c^1\Sigma_u^-–X^3\Sigma_g^-)$ Herzberg II bands, were observed for the first time in the Venera 9 and 10 data (Krasnopolsky et al., 1977). Successive laboratory experiments (Lawrence et al., 1977; Slanger, 1978) made this assignment. Moreover, a second weaker progression was recognized in the Venera 9 data, and assigned to the $O_2(A'^3\Delta_u–a^1\Delta_g)$ Chamberlain system (Slanger and Black, 1978).

The reported intensities for these two band systems were 2–3 kR ($1R = 10^6$ photon cm^{-2} s^{-1} $(4\pi$ ster$)^{-1}$) for the entire $O_2(c^1\Sigma_u^-–X^3\Sigma_g^-)$ 0–v'' progression in the Venera measurements and about 15 times less for the $O_2(A'^3\Delta_u–a^1\Delta_g)$ 0–v'' progression (Krasnopolsky, 1983). Similar values for the Herzberg II band progression were reported by Bougher and Borucki (1994) from the Pioneer Venus Orbiter data.

From ground-based observations, a few rotational lines belonging to the (0–10) Herzberg II band were identified in observations with the Keck I and Apache Point Observatory telescopes by Slanger et al. (2001, 2006), during an observation campaign to detect the $O^1S–^1D$ green line of atomic oxygen.

More recently, a Herzberg II series of bands was observed using the visible channel of VIRTIS (Visible and InfraRed Thermal Imaging Spectrometer), the imaging spectrometer on board the European mission to Venus, Venus Express. By averaging thousands of spectra acquired using the instrument in limb-mode observation, the 0–v'' progression was clearly detected on the night side of the planet (García-Muñoz et al., 2009). A total limb intensity of 128.4 kR was reported by the authors for the summed intensity of the v'' = 6–11 bands. Due to the weakness of these bands, the vertical profile was difficult to derive in the available data. However it was pointed out that the emission intensity was stronger at about 95 ± 1 km height, as shown in Figs. 4 and 5 in García-Muñoz et al. (2009).

* Corresponding author. Fax: +39 0645488188.
E-mail addresses: Alessandra.Migliorini@iaps.inaf.it (A. Migliorini), Giuseppe.Piccioni@iaps.inaf.it (G. Piccioni), JC.Gerard@ulg.ac.be (J.C. Gérard), lauriane.soret@ulg.ac.be (L. Soret), tom.slanger@sri.com (T.G. Slanger), Romolo.Politi@iaps.inaf.it (R. Politi), m.snels@isac.cnr.it (M. Snels), pierre.drossart@obspm.fr (P. Drossart), Fabrizio.Nuccilli@iaps.inaf.it (F. Nuccilli).

0019-1035/$ - see front matter © 2012 Elsevier Inc. All rights reserved.
http://dx.doi.org/10.1016/j.icarus.2012.11.017

The Herzberg II band system is not detected in the high resolution nightglow spectra of the Earth (Cosby et al., 2006), while emission lines of the c → b band system, which originates from the $O_2(c^1\Sigma_u^-)$ state, are detected (Slanger et al., 2003). By combining laboratory studies and airglow observations of the terrestrial planets, it was deduced that there exists a strict dependence between the $(c^1\Sigma_u^- - X^3\Sigma_g^-)$Herzberg II/$(A^3\Sigma_u^+ - X^3\Sigma_g^-)$Herzberg I and the [M]/[O] ratios (Slanger and Copeland, 2003). In the case of Venus and Mars M is CO_2, while for the Earth it is N_2. According to the concentrations of CO_2, N_2 and O in the atmospheres of the three terrestrial planets at the nightglow altitudes, the [M]/[O] ratio explains the presence of an intense Herzberg II emission on Venus and its absence on the Earth (Greer and Murtagh, 1985; Slanger and Copeland, 2003).

Although the $(A^3\Sigma_u^+ - X^3\Sigma_g^-)$ Herzberg I and $(A'^3\Delta_u - X^3\Sigma_g^-)$ Herzberg III systems are not ruled out in the Venus' atmosphere, the expected intensities are very low. The Herzberg I system is expected to be about 20 times less intense than the Herzberg II in the Venus' atmosphere, according to Krasnopolsky (1983). Considering the VIRTIS spectral sampling, it is hard to separate them from the Herzberg II bands. Hence it is not possible to unambiguously identify any feature belonging to the Herzberg I and III systems from VIRTIS data. In addition, at wavelengths shorter than 400 nm the stray light contribution is strong and the instrument sensitivity is not sufficient for weak band detection. As a consequence, the spectral region 300–400 nm must be treated with caution.

An extension of the previous work by García-Muñoz et al. (2009) concerning the O_2 nightglow emissions in the Venus atmosphere is provided in the present paper by using VIRTIS/Venus Express data acquired during a recent observing campaign at limb. Details of selected data, and data processing are reported in Section 2. Using the new observing mode, a better coverage of the altitude region around 95 km, where the Herzberg II band emissions are known to occur, is obtained. It has also allowed derivation of the vertical profile for the detected bands. In addition, for limb data acquired in March 2007 and April 2008, it was possible to simultaneously investigate the nightglow O_2 emissions in the visible and the IR Atmospheric band at 1.27 μm. Results are discussed in Section 3.

2. Observations with VIRTIS-M on Venus Express

The VIRTIS (Visible and InfraRed Thermal Imaging Spectrometer) instrument on board Venus Express is an imaging spectrometer composed of two channels. One, called M, covers the range from 0.3 to 5.1 μm using 864 bins, called bands, and has imaging capabilities, while the second, called H, has a higher spectral resolution but no imaging capabilities. In this study, we describe results obtained with data acquired with the M-channel of VIRTIS. The M-channel can cover the visible spectral range from 0.3 to 1.1 μm by steps of about 2 nm, while the IR part is sampled with ~10 nm steps. The VIRTIS-M spectrometer can operate both in nadir and limb modes. Because of the orbital configuration, the nadir mode observation is typically used in the ascending branch of the orbit, while the limb observations are concentrated when the spacecraft is near pericenter. As a consequence, the southern hemisphere of Venus is better mapped with nadir observations, while the limb observations preferentially sound the northern hemisphere. A detailed description of the instrument is reported in Drossart et al. (2007) and Piccioni et al. (2007).

For faint emissions such as those discussed in the present work, limb mode observations are the most suitable, as the signal is amplified by a factor of ~50 compared to nadir observations because of the long path in the line of sight through the atmosphere. A campaign of limb observations has been recently conducted, using the so-called "limb-tracking" technique. This technique takes advantage of the VIRTIS internal mirror capability to span the vertical direction. The *z*-axis of the instrument points at a fixed altitude, usually at 100 km or 120 km, depending on the distance of the spacecraft from the Venus north pole, and the VIRTIS image is built up by a sequence of scans at different altitudes, using the motion of the internal mirror of the spectrometer. The major innovation is that the limb altitude is kept fixed while the spacecraft moves along its orbit. This makes it possible to obtain a better sampling of a restricted altitude region, although the coverage of each single image is limited in latitude and local time. Data with an exposure time of 18 s have been used, in order to have a good signal to noise ratio (SNR). Details of the data are reported in Table 1.

The available data cover a restricted area around the anti-solar point as a consequence of the limb-tracking observing mode, as explained above. Owing to the limited coverage, an investigation of the O_2 emissions behavior with latitude cannot be carried out at this stage in the visible spectral range but the observations are progressing in the course of the mission.

Data have been calibrated applying a pipeline consolidated during the 5 years of the mission and outlined below. Data, originally in digital number (DN), are first of all initialized in order to identify the best parameters for the subsequent processes. Dark frames, acquired each 20 lines in a scientific image, are identified, analyzed in order to obtain the thermal evolution law of the observations, and removed. Then corrections for thermal evolution, bad frames, dead and saturated pixels, all known as the pre-processing stage, are applied. In the calibration stage, digital numbers are converted to radiance using the VIRTIS Instrument Transfer Function (ITF), and finally a post-processing stage is applied, in order to remove spikes and attenuate the detector non-uniformity response due to differences of responsivity between adjacent rows or columns. This stage includes also the spectral registration, which allows assigning a wavelength value to each band, according to a linear relation between wavelength and detector temperature derived from the internal calibration of the instrument, acquired during different mission phases (Cardesín Moinelo et al., 2010).

About 8700 spectra in the altitude range 90–120 km were selected in total. The spectrum, obtained by averaging the selected spectra, is shown in Fig. 1.

The Herzberg II is the prominent system observed on the night side upper mesosphere of Venus in the visible range. Eight bands of the (0–v'') progression clearly stand out above the noise; the (0–6) band at 422 nm, (0–7) at 450 nm, (0–8) at 480 nm, (0–9) at 514 nm, (0–10) at 552 nm, (0–11) at 594 nm, (0–12) at 641 nm, and (0–13) at 702 nm. The continuum is estimated to be less than 10% of the band intensities. In addition, three bands, centered at 558 nm, 604 nm, and 657 nm are also observed close to the Herzberg II bands. They have been identified as the (0–6), (0–7), and (0–8) transitions of the Chamberlain system.

In the following section, we discuss the vertical profile and intensity for the most intense bands of the Herzberg II and Chamberlain systems.

3. Results

An estimate of the tangent altitude of the Herzberg II bands was reported by García-Muñoz et al. (2009), although a direct measure of individual limb profiles was quite difficult because of the low SNR. Owing to the refined limb observing technique with VIRTIS, described above, we were able to derive the tangent profile of the emissions.

In the present study, the (0–7), (0–8), (0–9), (0–10), and (0–11) Herzberg II bands are considered. The other bands, though unambiguously detected on the averaged spectrum, have a low SNR

Please cite this article in press as: Migliorini, A., et al. The characteristics of the O_2 Herzberg II and Chamberlain bands observed with VIRTIS/Venus Express. Icarus (2012), http://dx.doi.org/10.1016/j.icarus.2012.11.017

Table 1
List of VIRTIS data used in the present work.

Limb session	Jtime	Latitude	Local time	Peak (km)	Intensity (kR)	FWHM (km)
1288-05 (∗)	2455134.6	0.5–13.5S	23–0.2 h	94.9	76	
1290-04 (†)	2455136.6	0.5–13.5S	23.5–0.5 h	94.2	132	
1292-04 (∗)	2455138.6	0–13.5S	23.7–0.6 h	96.1	89	10.2
1374-07 (∗)	2455220.8	4–14.5S	20.1–20.8 h	94.8	76	11.5
1375-06	2455221.8	3.5–14.5S	20–21 h	93.0	116	12.7
1377-03 (∗)	2455223.8	3.5–14.5S	20.4–21 h	95.7	72	
1426-05	2455272.7	3–11S	22–23 h	98	97	7.1
1428-04	2455274.7	3–11S	22–23 h	97.2	84	16.3
1774-12	2455620.7	1S–10N	0.5–1 h	93.5	96	9.5
1774-14	2455620.7	3–15N	0.2–1 h	92.7	110	16.6
1914-03 (∗)	2455760.6	28–33N	0–1.3 h	94.9	83	13.3
Data both in the visible and IR ranges						
317-06	2454163.8	11–30N	0.1–0.7 h	94.7	111	8.8
317-07 (∗)	2454163.8	23–44N	0–0.4 h	95.5	65	8.9
323-07 (∗)	2454169.8	25–50N	0.4–1 h	96.2	53	8.2
324-06 (∗)	2454170.8	11–30N	0.7–1.5 h	95.1	91	16.5
324-07 (∗)	2454170.8	23–50N	0.5–1.2 h	95.8	57	9.7
327-06 (∗)	2454173.8	25–50N	1–1.5 h	94.6	27	
715-02	2454561.7	5S–9N	22.5–23.3 h	98	92	11.2

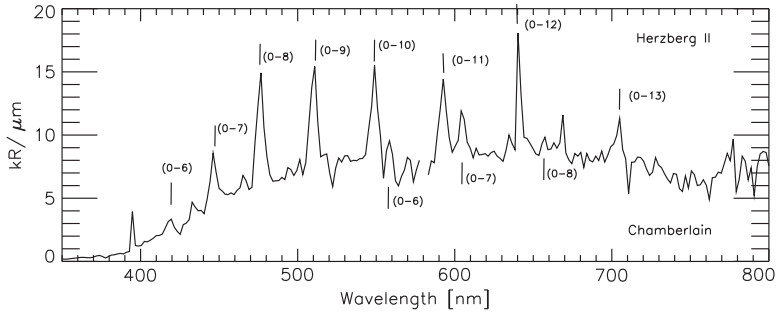

Fig. 1. Average spectrum of VIRTIS in the 350–800 nm spectral range. The identified Herzberg II and Chamberlain transitions are labelled by the (0–v'') labels above and below the spectrum line, respectively.

which does not allow further investigation. For each band, the radiance was first converted into Rayleigh units (Baker, 1974). The radiance was then integrated considering the wavelength ranges 446–459 nm for the (0–7) band, 476–484 nm for (0–8), 511–518 nm for (0–9), 548–556 nm for (0–10), and 592–596 nm for the (0–11) band, respectively. The continuum was estimated following the method described in Soret et al. (2010). The continuum is likely due to infield stray light due to scattering of thermal emission by haze from nearby atmospheric windows. To remove this contribution, a first order polynomial fit is applied above 105 km and below 90 km. Soret et al. (2010) argued that the applied method works well for bright emissions, while the continuum contribution is difficult to estimate in the case of weak emissions. In the visible spectral range where the detected emissions are weak, we consider the integrated emission of the Herzberg II system, instead of using single bands, in order to have a higher SNR and hence a better definition of the emission. The boundaries at 105 and 90 km do not work well with the Chamberlain bands, which are fainter than the Herzberg II bands; hence, ad hoc boundaries were adopted in this case. Spectra were selected in the altitude range 90–120 km, for each acquired VIRTIS image, and divided into 3-km bins. Spectra in each altitude bin were averaged and displayed versus altitude. Fig. 2 illustrates examples of the mean intensity distribution for four observed limb profiles. These images have been selected in different periods of the mission, in order to verify also the variability of the Herzberg II bands with time.

During these observations, the spatial resolution varied from 1 km, in the limb-tracking mode, to 2.5 km for the tangential limb observations. In order to avoid spurious features in the case of weak emissions and have an homogeneous vertical resolution, we use a bin resolution of 3 km for all the analyzed data. This is also the uncertainty associated with the peak altitude derived for the tangent vertical profiles.

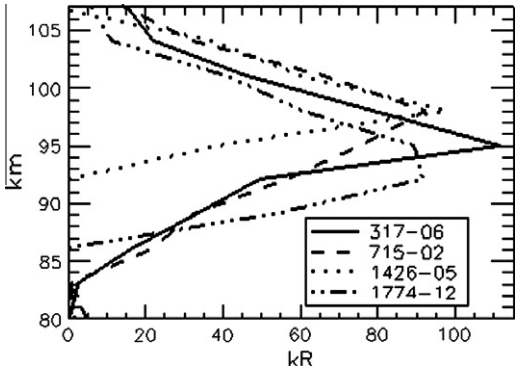

Fig. 2. Examples of tangent profiles of the Herzberg II system. They are identified by the corresponding VIRTIS orbit number and session, as reported in Table 1. They are obtained by considering the contribution of the single bands with v'' = 7–11 of the system. The continuum is estimated as described in Soret et al. (2010). The uncertainty in the position is assumed to be equal to 3 km, that is the vertical bin size.

In addition, we consider the limb profile of the integrated band system, as we previously verified that each band peaked at the same altitude, as required, within the estimated errors.The limb profiles were then fitted with a Gaussian curve to estimate the

Please cite this article in press as: Migliorini, A., et al. The characteristics of the O_2 Herzberg II and Chamberlain bands observed with VIRTIS/Venus Express. Icarus (2012), http://dx.doi.org/10.1016/j.icarus.2012.11.017

peak altitude, the intensity at peak, and the full width at half maximum (FWHM). The tangent altitude is in the range 92.7–98 km, with a FWHM ranging from 7.1 to 16.5 km. However, for some images, the SNR is very low and the fit with the Gaussian curve is difficult. For these cases, namely the 327-06, 1288-05, 1290-04, 1377-03, the FWHM is not derived. Considering the other cases, the FWHM is equal to 11.5 ± 3.2 km on average.

The intensities, reported in Table 1, are quite variable. In some cases, marked with a star, the Herzberg II progression is only partly detectable. For these cases, the reported intensity is not representative because the contribution from some bands is missing, and hence not included in the discussion. In the case of image 1290-04, marked with (†) in Table 1, the total intensity is overestimated, because of problems in the definition of the (0–9) transition band. This image is not included in the discussion. In the present work, we consider as representative intensities only those data where the (0–7) up to the (0–11) bands were simultaneously detected. For these cases, the total integrated intensity along the line of sight ranges between 84 kR and 116 kR. Considering the intensity factor at limb equal to 50, as mentioned in Section 2, the observed Herzberg II intensities are in good agreement with the values reported in the Venera data (Krasnopolsky, 1983). The uncertainty on the absolute intensity of the single measurements is estimated to be on the order of 20%. The peak altitude of the emission is not variable from one band to the other, as mentioned above. Hence, although in several cases the complete progression is not observed, we can derive a statistical behaviour of the peak altitude of the Herzberg II observed bands, as shown in Fig. 3.

The mean value of the peak position is 95.5 ± 1.6 km, which coincides also with the weighted average. Despite the low number of profiles where the emissions in the visible spectral range can be studied, the distribution shows several similarities with the characteristics of the (0–0) O_2 IR atmospheric band (Piccioni et al., 2009). In that case, the statistical distribution of the peak position in the case of the (0–0) O_2 band was discussed, as retrieved with the onion peeling technique. The mean value in the case of the tangent peak altitude was also reported, equal to 95 ± 2.4 km. The comparison between the Herzberg II and the (0–0) O_2 band is discussed in detail in Section 3.2, where simultaneous observations in the visible and IR are presented.

3.1. Chamberlain system

Three bands of the Chamberlain system were also detected. They correspond to the 0–v'' progression with v'' = 6, 7, 8, centered at 558 nm, 604 nm, and 657 nm. However, because of the low SNR at wavelengths longer than 640 nm, we were able to investigate the limb profile only for the (0–6) and (0–7) bands. In the images named 1426-05 and 1774-12 in Table 1, the two bands are well defined. In the case of image 1426-05, the intensities are equal to 9.8 kR and 10.3 kR respectively for the (0–6) and (0–7) bands, while in the image 1774-12 the intensities are 6.8 kR and 8.6 kR for the same bands (see Fig. 4). The intensity ratio $I(0–7)/I(0–6)$ is estimated to be 1.05 and 1.27 for the two images respectively; these values are in a good agreement with the theoretical intensity ratio of 1.28 (Bates, 1989). However, a better statistics is required to derive firm conclusions. The total integrated intensity profile, obtained considering the (0–6) and the (0–7) bands of the Chamberlain system from image 1774-12, is shown with a dashed line in Fig. 4 as an example.

The profile of the Chamberlain bands is also compared to the total intensity of the Herzberg II system measured simultaneously. It appears that the Chamberlain system peaks a few km higher than the Herzberg II system, though this is less evident in the case of image 1426-05. This behaviour is discussed in relation with a one-dimensional model applied to these observations (Gérard et al., 2012). Unfortunately, the statistics of the Chamberlain bands is very poor, as a consequence of the weakness of these bands and also to their vicinity to the Herzberg II bands. Hence, it is quite difficult to separate them from the background in most of the available data.

According to the Venera observations, the Chamberlain band emissions are on average 13 times less intense than the Herzberg II bands (Krasnopolsky, 1983). In the observed cases, the Chamberlain (0–6) and (0–7) bands are respectively 10 times and 9.4 times less intense than the integrated Herzberg II system intensity, considering a peak intensity of 97 kR for the image 1426-05, while they are 14.1 times and 11.1 times less intense than the Herzberg II system intensity, assuming a peak intensity of 96 kR for the Herzberg II system, for the image 1774-12. However, we must take into account that these values only refer to two bands of the Chamberlain system.

Concerning the peak altitude, according to Krasnopolsky's model (2011), the Chamberlain system has a maximum of emission at 110 km. In the VIRTIS data, we find that the Chamberlain bands emissions occur at about 100 km tangent height. Considering the difference between the tangent height and the altitude of the Volume Emission Rate, the former being 2–5 km lower than the latter, we can conclude that there is quite good agreement between the expected altitude from this model and our results, in particular that the Chamberlain system lies above the Herzberg II one. This is further confirmed by an ad hoc one-dimensional atmospheric model developed to interpret our results, based on neutral densities derived from Venus Express remote sensing observations. A brief discussion of the model and its conclusions is reported in Section 4, while a more detailed description of the model can be found

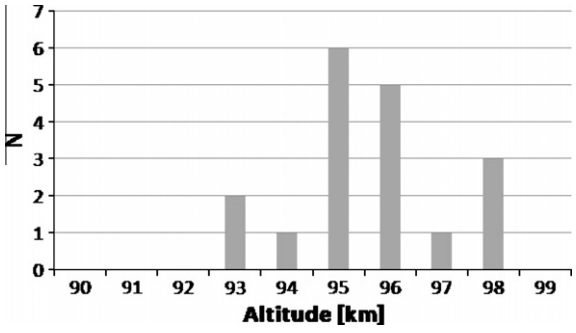

Fig. 3. Statistical distribution of the Herzberg II peak altitude, acquired in the period from 2007-03-04 to 2011-07-18. The mean value of the peak position is 95.5 ± 1.6 km, which corresponds also to the weighted average.

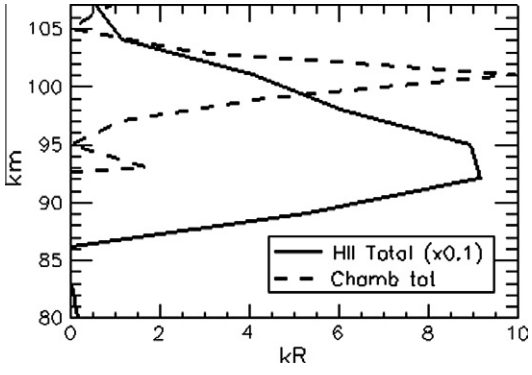

Fig. 4. Tangent profile of the integrated intensity obtained by considering the (0–6) and the (0–7) bands of the Chamberlain system, compared to the tangent profile of the Herzberg II band system. The example refers to the VIRTIS image 1774-12 acquired on 2011-02-28.

Please cite this article in press as: Migliorini, A., et al. The characteristics of the O_2 Herzberg II and Chamberlain bands observed with VIRTIS/Venus Express. Icarus (2012), http://dx.doi.org/10.1016/j.icarus.2012.11.017

in Gérard et al. (2012). Noteworthy the results reported here are the first observations of the Chamberlain emission altitude profiles at Venus.

3.2. Comparison with O_2 infrared emissions

Details of the data included in this investigation are listed in Table 1. Data were acquired in the period from 2007-03-04-03 to 2011-07-18. For the data acquired from 2007-03-04 to 2008-04-05, reported in the lower part of Table 1, both visible and IR spectra are available. The cases shown are the best ones where the 0–v'' progression of the Herzberg II bands are clearly observed. This might be because the O_2 airglow emissions were stronger than in the other cases, or because the SNR was good. For these data, a direct comparison of the O_2 nightglow emissions in the visible and IR ranges in the Venus atmosphere is possible. Only two cases of direct comparison between visible and IR nightglow emissions are shown in Fig. 5 as an example. Data were acquired on 2007-03-04 (Fig. 5a) and 2008-04-05 (Fig. 5b). However, a few other cases, where simultaneous O_2 nightglow emissions in the visible and IR are detected, were analyzed and listed in Table 1.

The intensity of the O_2 emission in the IR was scaled by a factor of 0.002, in order to have the two curves in the same plot. A good agreement between the peak altitude of the Herzberg II and the (0–0) emission peak of the $O_2(a^1\Delta_g{-}X^3\Sigma_g^-)$ is found, as seen in Figs. 5a and b. For the particular cases analyzed in this work, the Herzberg II system intensity is about 500 times less intense than the $O_2(a^1\Delta_g{-}X^3\Sigma_g^-)$ (0–0) band in the infrared.

For the seven images listed in the lower part of Table 1, where the IR and visible spectra were acquired simultaneously, we compare the peak altitude at limb for the two spectral ranges (Fig. 6). The same trend of the peak altitude fluctuation is observed in the IR and visible. The peak positions are compatible within the statistical errors, for the IR (0–0) band and the Herzberg II bands, though the latter peak is on average slightly lower than the (0–0) band. On average, the (0–0) emission peak of the $O_2(a^1\Delta_g{-}X^3\Sigma_g^-)$ is observed at 97.4 ± 2.5 km, as reported in the statistical study of this emission in Piccioni et al. (2009), based on VIRTIS/Venus Express data, and the relative peak position at limb is on average at 95 ± 2.4 km. The FWHM is variable with latitude, ranging from 11 km at equator to 6 km at mid-high latitudes (Piccioni et al., 2009). In the case of the Herzberg II bands, the peak emission is observed at about 95–96 km in limb view, while the FWHM is wider than the mean value for the IR emission bands. Considering the high variability of this parameter and the limited sampling in latitude of the data in the visible range, which are concentrated close to equator where the FWHM is equal to 11 km in the IR, a similar value for the FWHM is found. The average trends are in good agreement. However, the behavior with respect to latitude in the case of the Herzberg II bands cannot be investigated at this time because of an insufficient coverage at high latitudes.

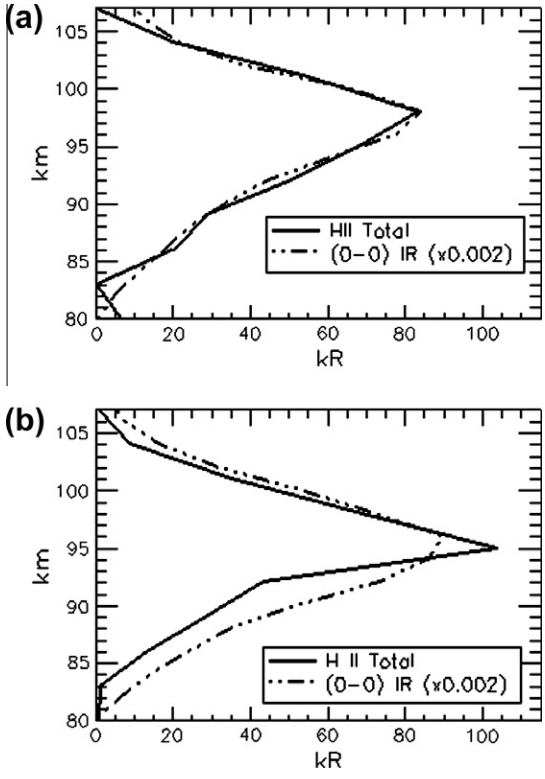

Fig. 5. (a) Comparison between the vertical profile of the O_2 emissions in the IR at 1.27 μm and in the visible range. The intensity of the emission in the IR was scaled to a factor 0.002, in order to make easier the comparison with the Herzberg II bands intensity and have the two profiles in the same plot. The IR and visible spectra are simultaneously acquired on 2007-03-04 (image number 317-06). (b) The same for the VIRTIS images acquired on 2008-04-05 (image number 715-02).

4. One-dimensional simulations

The results reported here allow refining the modelling of the Venus nightside airglow. Based on the recent VIRTIS observations of the O_2 nightglow emissions, both in the visible and infrared spectral regions, it is possible to constrain the production and collisional deactivation of excited O_2 molecules. The model is based on a steady state equation for the population of the upper state of the transition (Gérard et al., 2012). The atomic oxygen and CO_2 densities used in the model are taken from previous VIRTIS and SPICAV measurements (Soret et al., 2012). According to this calculation, the peak position of the Herzberg II bands is located slightly lower than the peak position for the $a^1\Delta$ (0–0) band in the IR, as it is observed in the simultaneous VIRTIS data in the visible and IR (see Fig. 6). The Chamberlain bands are predicted to peak about 4 km higher than the Herzberg II bands. This confirms the few VIRTIS observations where the altitude of the Chamberlain bands may be measured, a consequence of the faintness of these emissions (see Fig. 4). The 4–5 km altitude difference between the Infrared Atmospheric and the Herzberg II bands on one hand, and the Chamberlain bands on the other hand, is presumed to be a consequence of smaller quenching rate coefficients for the a and c singlet states compared to more efficient deactivation of the A′ triplet state by CO_2 molecules and O atoms.

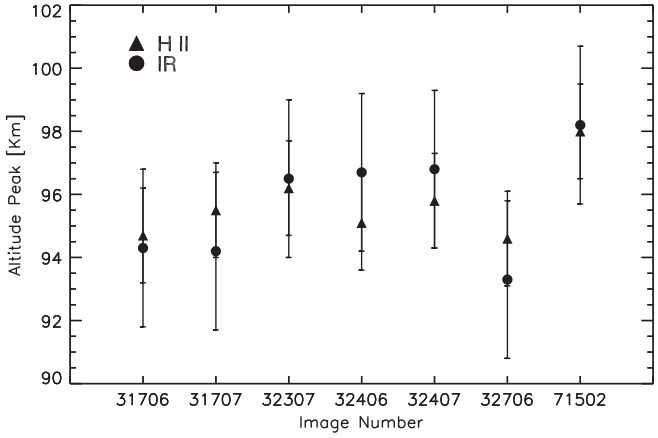

Fig. 6. Peak altitude at limb for the Herzberg II integrated band system (marked with a triangle), as derived in this work, compared to the peak altitude of the (0–0) emission of the $O_2(a^1\Delta_g{-}X^3\Sigma_g^-)$ (marked with a round symbol), from Piccioni et al. (2009).

A comparison between observed and predicted relative intensities shows that the model is able to reproduce the relative intensities of the Herzberg II and the (0–0) IR Atmospheric transition satisfactorily, while the agreement between model and observations is worse for the Chamberlain bands, possibly due to the limited number of observations.

5. Conclusions

We report the detection of eight bands of the O_2 Herzberg II and three bands of the Chamberlain systems in the visible spectral range, observed by the VIRTIS spectrometer on board Venus Express.

The good sampling in the altitude range of about 90–120 km, achieved with the limb-tracking technique, allows investigation of the vertical profile of the detected bands. We found that the two systems peak at different altitudes. In particular, the Chamberlain bands peak about 4 km higher than the Herzberg II bands. This trend is well reproduced in the emission model developed using oxygen and CO_2 profiles retrieved from Venus-Express observations.

The integrated intensity of the Herzberg II system, with $v'' = 7$–11, varies in the range 84–116 kR, in agreement with the previous detection by García-Muñoz et al. (2009). For the Chamberlain system, only two bands, namely (0–6) at 558 nm, and (0–7) at 604 nm were investigated in this work. For these bands, the relative intensity ratio $I(0–7)/I(0–6)$ has been calculated and compared with the theoretical value, equal to 1.28. The results are in reasonable agreement with theory. The (0–6) Chamberlain band falls very close to the so-called atomic oxygen green line, which occurs at 557.7 nm. However, no indication of the latter has been found in the VIRTIS data so far. This could be a consequence of the faintness or the sporadic presence of the oxygen green line, or this could be explained by the fact that the altitude we are considering for the Chamberlain band detection is not where the green line emission occurs, which is still debated. A further investigation of the VIRTIS data at limb might shed more light on the green line detection.

The results presented allow us to improve our knowledge about the minor species in the Venus atmosphere. With the information derived from the vertical profiles of these band systems, we have a great improvement of the knowledge of the vertical structure and hence of the dynamical properties of the night side atmosphere of Venus. Moreover, the Chamberlain bands, peaking at an altitude different from Herzberg II and the IR atmospheric bands, allows tracing of the day-to-night circulation at different altitudes, leading to a 3-D structure of the atmosphere, as has already been done, by combining the ultraviolet NO and IR O_2 emissions (Gérard et al., 2009).

Acknowledgments

The authors thank ESA, ASI, CNES and all the national space agencies which support Venus-Express. AM is supported by ASI (Grant: ASI-INAF I/050/10/0). TGS supported by NASA Planetary Atmospheres Grant NNX08AO27G. Partial funding for this research was provided by the PRODEX program of the European Space Agency, managed in collaboration with the Belgian Federal Science Policy Office.

References

Baker, D.J., 1974. Rayleigh, the unit for light radiance. Appl. Opt. 13, 2160–2163.
Bates, D.R., 1989. Oxygen band system transition arrays. Planet. Space Sci. 37, 881–887.
Bougher, S.W., Borucki, W.J., 1994. Venus O_2 visible and IR nightglow: Implications for lower thermosphere dynamics and chemistry. J. Geophys. Res. 99, 3759–3776. http://dx.doi.org/10.1029/93JE03431.
Cardesín Moinelo, A., Piccioni, G., Ammannito, E., Filacchione, G., Drossart, P., 2010. Calibration of hyperspectral imaging data: VIRTIS-M onboard Venus Express. IEEE Trans. Geosci. Remote Sens. 48, 3941–3950.
Cosby, P.C., Sharpee, B.D., Slanger, T.G., Huestis, D.L., Hanuschik, R.W., 2006. High-resolution terrestrial nightglow emission line atlas from UVES/VLT: Positions, intensities, and identifications for 2808 lines at 314–1043 nm. J. Geophys. Res. 111, A12307.
Drossart, P. et al., 2007. Scientific goals for the observation of Venus by VIRTIS on ESA/Venus Express mission. Planet. Space Sci. 55, 1653–1672.
García-Muñoz, A., Mills, F.P., Slanger, T.G., Piccioni, G., Drossart, P., 2009. Visible and near-infrared nightglow of molecular oxygen in the atmosphere of Venus. J. Geophys. Res. 114, E12002. http://dx.doi.org/10.1029/2009JE003447.
Gérard, J.C. et al., 2009. Concurrent observations of the ultraviolet nitric oxide and infrared O_2 nightglow emissions with Venus Express. J. Geophys. Res. 114, E00B44.
Gérard, J.C., Soret, L., Migliorini, A., Piccioni, G., 2012. Oxygen nightglow emissions of Venus: Vertical distribution and role of collisional quenching. Icarus. http://dx.doi.org/10.1016/j.icarus.2012.11.019.
Greer, R.G.H., Murtagh, D.P., 1985. Singlet oxygen nightglow in the atmosphere of Earth, Venus and Mars. In: Proceedings of Galway A.S.G.I. Meeting.
Krasnopolsky, V.A., 1983. Venus spectroscopy in the 3000–8000 Å region by Veneras 9 and 10. In: Hunten, D.M. et al. (Eds.), Venus. Univ. of Ariz. Press, Tucson, pp. 459–483.
Krasnopolsky, V.A., 2011. Excitation of the oxygen nightglow on the terrestrial planets. Planet. Space Sci. 59, 754–766.
Krasnopolsky, V.A., Krysko, A.A., Rogachev, V.N., Parshev, V.A., 1977. Spectroscopy of the night-sky luminescence of Venus from the interplanetary spacecraft Venera 9 and 10. Cosmic Res. 14, 687–692.
Lawrence, G.M., Barth, C.A., Argabright, V., 1977. Excitation of the Venus night airglow. Science 195, 573–574.
Piccioni, G. et al., 2009. Near-IR oxygen nightglow observed by VIRTIS in the Venus upper atmosphere. J. Geophys. Res. 114, E00B38. http://dx.doi.org/10.1029/2008JE003133.
Piccioni, G. et al., 2007. VIRTIS: The Visible and Thermal Imaging Spectrometer. ESA-SP 1295, ESA Publications Division, Noordwijk, The Nederlands.
Slanger, T.G., 1978. Generation of $O_2(c^1\Sigma_u^-, C^3\Delta_u, A^3\Sigma_u^+)$ from oxygen atom recombination. J. Chem. Phys 69, 4779–4791.
Slanger, T.G., Black, G., 1978. The $O(^1S)$ airglow – new laboratory results. In: Kurylo, M.J., Braun, W. (Eds.), 12th Informal conference of Photochemistry, Gaithersburg, MD, USA, 28 June–1 July 1976. Natl. Bur. Standards, Washington, DC, USA, pp. 102–104.
Slanger, T.G., Copeland, R.A., 2003. Energetic oxygen in the upper atmosphere and the laboratory. Chem. Rev. 103, 4731–4765.
Slanger, T.G., Cosby, P.C., Huestis, D.L., Bida, T.A., 2001. Discovery of the atomic oxygen green line in the Venus night airglow. Science 291, 463–465.
Slanger, T.G., Cosby, P.C., Huestis, D.L., 2003. A new O_2 band system: The $c^1\Sigma_u^- – b^1\Sigma_g^+$ transition in the terrestrial nightglow. J. Geophys. Res. 108 (A2), 1089. http://dx.doi.org/10.1029/2002JA009677.
Slanger, T.G., Huestis, D.L., Cosby, P.C., Chanover, N.J., Bida, T.A., 2006. The Venus nightglow: Ground-based observations and chemical mechanism of the oxygen airglow. Icarus 182, 1–9.
Soret, L., Gérard, J.C., Piccioni, G., Drossart, P., 2010. Venus OH nightglow distribution based on VIRTIS limb observations from Venus Express. Geophys. Res. Lett. 37, L06805. http://dx.doi.org/10.1029/2010GRL042377.
Soret, L., Gérard, J.C., Montmessin, F., Piccioni, G., Drossart, P., Bertaux, J.L., 2012. Atomic oxygen on the Venus nightside: Global distribution deduced from airglow mapping. Icarus 217 (2), 849–855.